Am J Cancer Res 2023;13(11):5306-5319
www.ajcr.us /ISSN:2156-6976/ajcr0148931

Original Article

A risk model based on ferroptosis- and cuproptosis-related lncRNAs predicts prognosis and immune microenvironment in lung adenocarcinoma by bioinformatics analysis and experimental verification

Xiaoying Xu[1,2*], Xinzhi Feng[3*], Pengju Zhang[4], Xiaoyan Lin[1,2]

[1]College of Basic Medicine, Shandong First Medical University-Shandong Academy of Medical Sciences, Jinan, Shandong, China; [2]Department of Pathology, Shandong Provincial Hospital Affiliated to Shandong First Medical University, Jinan, Shandong, China; [3]Department of Radiology, Shandong Provincial Hospital Affiliated to Shandong First Medical University, Jinan, Shandong, China; [4]Department of Biochemistry and Molecular Biology, School of Basic Medical Sciences, Cheeloo College of Medicine, Shandong University, Jinan, Shandong, China. [*]Equal contributors.

Received January 4, 2023; Accepted September 29, 2023; Epub November 15, 2023; Published November 30, 2023

Abstract: Ferroptosis and cuproptosis are both novel types of cell death. Long noncoding RNAs (lncRNAs) are associated with multiple cancers. Notably, bioinformatics study of ferroptosis- and cuproptosis-related lncRNAs (FCLs) in lung adenocarcinoma (LUAD) has not been elucidated. In this study, we used univariate Cox, multivariate Cox, and least absolute shrinkage and selection operator Cox (LASSO-Cox) analyses to screen three FCLs, namely AC079193.2, AC090559.1, and AL512363.1. We then showed that these three FCLs were tumor-specific and correlated with ferroptosis and cuproptosis using qRT-PCR. Next, a prognostic risk model consisting of high- and low-risk cohorts was successfully constructed based on The Cancer Genome Atlas-LUAD data. The high-risk group consistently demonstrated poor prognosis. The accuracy of the model was evaluated using AUC, C-index curves, and nomograms. Furthermore, KEGG and GO analysis with R software showed significant enrichment in immune functions and metabolic pathways. Hereto, the immune function and immune cell expression results were more pronounced in the low-risk versus high-risk group. In conclusion, the prognostic risk model comprised of three FCLs effectively predicted patient outcomes and is associated with the immune microenvironment in LUAD.

Keywords: Bioinformatics analysis, lung adenocarcinoma, ferroptosis & cuproptosis-related lncRNA, risk model, prognosis, immune microenvironment

Introduction

As of 2022, lung cancer has the second-highest estimated incidence and the highest projected mortality among all cancers worldwide. It consists of two primary subtypes: non-small-cell lung cancer and small-cell lung cancer [1, 2]. Lung adenocarcinoma (LUAD) is a common histologic subtype of non-small-cell lung cancer, seen in non-smoking patients with driver gene mutations [3]. Despite many available treatments, the therapeutic outcomes for LUAD remain poor, and the 5-year survival probability remains relatively low, especially for patients with advanced cancer [4].

Ferroptosis, an iron-dependent type of cell death with abnormal metabolism and biochemical processes, was first reported by Dixon et al. in 2012 [5]. Unlike other forms of cell death such as apoptosis, autophagy, necroptosis, and pyroptosis, ferroptosis mainly involves a combination of iron toxicity, lipid peroxidation, and plasma membrane damage [6, 7]. Inducers of ferroptosis include various substances, including erastin, lanperisone, sorafenib, and artemisinin. For this study, erastin was selected as the primary inducer. Erastin triggers oxidative, iron-dependent cell death by reducing glutathione levels through direct inhibition of the cystine/glutamate antiporter system Xc-, leading to

the activation of the endoplasmic reticulum stress response [8].

Copper is a trace element essential for life in various biological processes in humans. It plays a dual role as a nutrient and a toxin [9]. Copper is directly involved in the tricarboxylic acid cycle and binds with lipoylated molecules to promote iron (Fe)-sulfur (S) cluster protein loss, ultimately leading to cell death [10]. Elesclomol is a potent copper ionophore, and when it binds to copper ions (elesclomol-Cu (II)), it rapidly transports Cu^{2+} to the mitochondria to induce a form of cell death known as cuproptosis [11]. Cuproptosis is novel cell death that differs from other well-documented forms such as apoptosis, necroptosis, pyroptosis, and ferroptosis [12].

Long noncoding ribonucleic acid (lncRNA), initially reported in 1991 [13], refers to a class of RNA molecules with a length > 200 nt. These lncRNAs are primarily located in the nucleus and are involved in biological processes, including cell cycle, metabolism, cellular drug resistance, immune microenvironment, and development of multiple malignant tumors [14, 15]. LncRNAs are strongly associated with many cancers, including LUAD [16]. However, ferroptosis- and cuproptosis-related lncRNAs (FCLs) in LUAD have not been reported.

Previous research has separately explored risk models related to cuproptosis and ferroptosis. However, a prognostic model that combines both cuproptosis and ferroptosis has not been investigated. Given the complex pathogenesis, high recurrence rate, and increased drug resistance associated with LUAD, it is imperative to conduct more theoretical research to advance the development of cutting-edge treatments in clinical practice. In this study, we successfully identified three FCLs that are tumor-specific and strongly associated with the processes of ferroptosis and cuproptosis. The expression patterns of these three FCLs were consistent across various datasets, including The Cancer Genome Atlas (TCGA) database, cell lines, and clinical tissue samples. Moreover, we have established a risk prognostic model based on TCGA data. We also assessed the correlation between this risk model and functional annotations, the immune environment, and drug sensitivity. This novel model can predict overall survival (OS) in patients and provides a theoretical foundation for the advancement of clinical treatments in LUAD.

Materials and methods

Data acquisition

Transcriptome data for LUAD, including 59 normal cases and 598 tumor cases, and corresponding clinical information were obtained from the TCGA database (http://portal.gdc.cancer.gov/). Cuproptosis-related genes (CRGs) were obtained in a previous study [17]. Ferroptosis-related genes (FRGs) were acquired from the FerrDb V2 database (www.zhounan.org/ferrdb/current/). Clinical tissues were collected from Shandong Provincial Hospital. The study was approved by the Ethics Committee of the Affiliated Shandong Province Hospital of Shandong First Medical University.

Identification of FCLs

Pearson's correlation algorithm was used to identify FCLs based on their associations with FRGs (|cor| > 0.2, P < 0.001) and CRGs (|cor| > 0.4, P < 0.001). The intersection of these two sets formed the FCL dataset, comprising 206 lncRNAs. The relationships between FCLs and FRGs, as well as CRGs, were analyzed using R. Univariate Cox (Uni-Cox) analysis was applied to screen prognosis-related FCLs (P < 0.05). The best prognosis-related FCLs were filtered using the least absolute shrinkage and selection operator Cox (LASSO-Cox) algorithm and multivariate Cox (multi-cox) analysis. Then, the TCGA-LUAD dataset was randomly categorised into two groups: a training group to construct the FCL signature and a test group for assessing its accuracy. The risk score for the FCL signature was calculated using a formula that considered the expressions of AC079193.2, AL5123663.1, and AC090559.1, each assigned a specific coefficient (i.e., expression AC079193.2*-1.72742139871253 + expression AL5123663.1*-0.29753666108855 + expression AC090559.1*-0.23143589070073).

Cell culture

The BEAS-2B, 95D, and A549 cell lines were gifted by Jiang Yifan, a senior researcher at Shandong First Medical University. The BEAS-2B cell line was cultured in Dulbecco's Modified Eagle Medium (Gibco, Billings, MT, USA) and

12% fetal bovine serum (FBS; Cell-box, Shenzhen, China), whereas 95D and A549 cell lines were cultured in RPMI 1640 (Gibco) and 12% FBS. All cell cultures were maintained at 37°C and 5% CO_2 in a cell incubator.

Quantitative real-time reverse transcription-polymerase chain reaction (qRT-PCR) analysis

Elesclomol and erastin were both procured from MCE (Monmouth Junction, NJ, USA). The medium was replaced after elesclomol (0 nM, 5 nM, 10 nM, 15 nM, 20 nM, and 25 nM) pulse treatment for 2 h in the presence of 1 μM copper (II) chloride or after erastin (0 μM, 5 μM, 10 μM, 15 μM, 20 μM, and 25 μM) treatment for 24 h, respectively. After 24 h, the total RNA was extracted using TRIzol (Tiangen, Beijing, China). Complementary deoxyribonucleic acid (cDNA) was obtained using the HisScript ® III 1st Strand cDNA Synthesis Kit (Vazyme, Nanjing, China). qRT-PCR was performed using the ChamQ Universal SYBR qPCR Master Mix (Vazyme). Finally, the $2^{-\Delta\Delta Ct}$ algorithm was applied to calculate relative FCL expression. Detailed primer information is presented in Supplementary Table 1.

Construction and examination of the risk prognostic model

The Kaplan-Meier method was used to determine the OS of patients in the two risk cohorts and across multiple clinical cohorts. The risk model accuracy and FCL prognostic value were validated using receiver operating characteristic (ROC) curves, area under the curve (AUC) analysis, C-index curve analysis, and principal component analysis (PCA). Additionally, the independent prognostic factors in the risk model were explored using Uni-Cox and Multi-Cox analyses. Finally, a nomogram was used to predict the 1-, 3-, and 5-year OS based on the risk model, and calibration was performed to test the accuracy of the nomogram prediction.

Gene ontology (GO) and Kyoto encyclopaedia of genes and genomes (KEGG) analyses

R software was employed for GO and KEGG (false discovery rate < 0.05) analyses between the two risk groups. The GO analysis comprises biological processes, cellular components, and molecular functions.

Analysis of the tumor immune microenvironment

R software was used to calculate the correlation between the two risk groups and immune-related function, immune check points, and m6A-related genes, respectively. Five methods, namely TIMER, CIBERSORT, CIBERSORT-ABS, QUANTISEQ, MCPCOUNTER, XCELL and EPIC, were used to explore the relationship between FCLs and immune cells in the two risk groups.

Statistical analysis

All bioinformatics-related figures were obtained by R (v4.1.3 and v4.2.1) software, while Perl (5.30.0.1) software was used for program execution. All experiment-related statistical graphs were drawn by GraphPad Prism (v9.0.0.121). Statistical significance was defined as p-value < 0.05 (*P < 0.05, **P < 0.01, ***P < 0.001).

Results

Screening of FCLs

The flowchart for the study is displayed in **Figure 1**. Coexpression analysis for LUAD was used to identify 1,096 ferroptosis-related lncRNAs (FRLs) and 668 cuproptosis-related lncRNAs (CRLs), with the common portion comprising 206 FCLs (**Figure 2A**). Uni-Cox analysis revealed 18 statistically significant FCLs (**Figure 2D**). Next, three CRLs were subjected to the LASSO-Cox analysis and multi-Cox analysis to determine the CRL characteristics (**Figure 2B**, **2C**). Heatmaps were generated to visualize the associations based on the Multi-Cox algorithm between FCLs (AC079193.2, AC090559.1, and AL512363.1) and FRGs (**Figure 2E**; Supplementary Table 2), as well as CRGs (**Figure 2F**; Supplementary Table 3).

Expression of FCLs

According to the TCGA database, tumor tissues exhibited lower expression of AC079193.2 and AC090559.1 compared with normal tissues, which was associated with a worse prognosis, while AL512363.1 expression showed the opposite trend (**Figure 3A-F**). The mRNA levels of these three FCLs were also detected in cell lines and clinical tissues via qRT-PCR, with a similar trend to the TCGA database (**Figure 3G**,

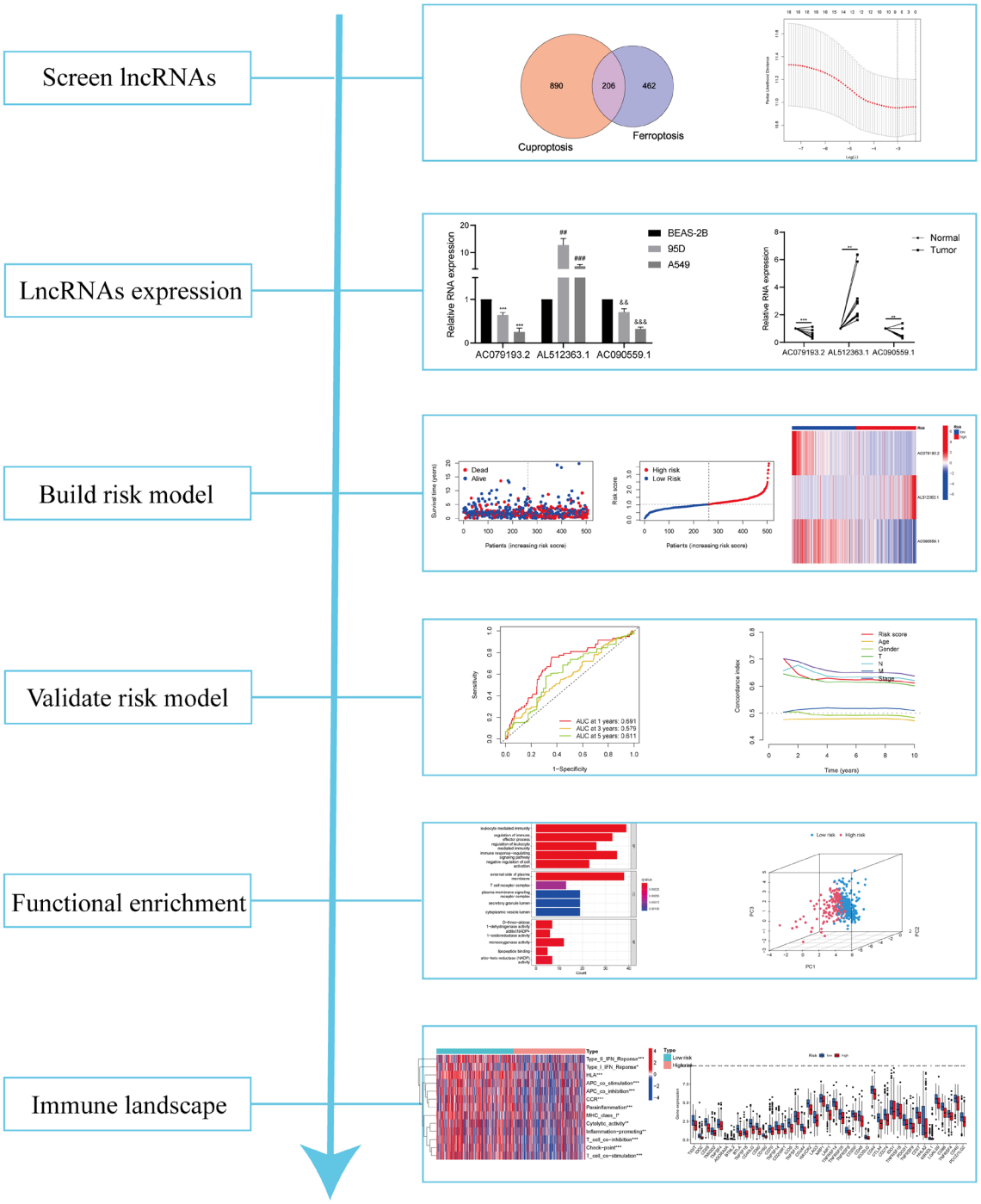

Figure 1. The flowchart of this study. Datasets were obtained from TCGA database. Pearson algorithm was used to screen FCLs. Subsequently, we detected levels of three FCL in cell lines and clinical tissues. Next, we established risk model and verified its accuracy. Then, functional analysis showed that multiple immune-related function was enriched. Finally, we conducted immune landscape, including immune function analysis and immune checkpoint.

3H). These levels were higher in the 95D cells than in the A549 cells. We used two drugs (erastin: 0, 5 μM, 10 μM, 15 μM, 20 μM, and 25 μM; elesclomol: 0, 5 nM, 10 nM, 15 nM, 20 nM, and 25 nM) to test the tolerance of cells. The CCK8 results showed that the 95D cells had higher resistance to both drugs than the A54 cells (**Figure 3I**, **3J**). We also examined FRG and

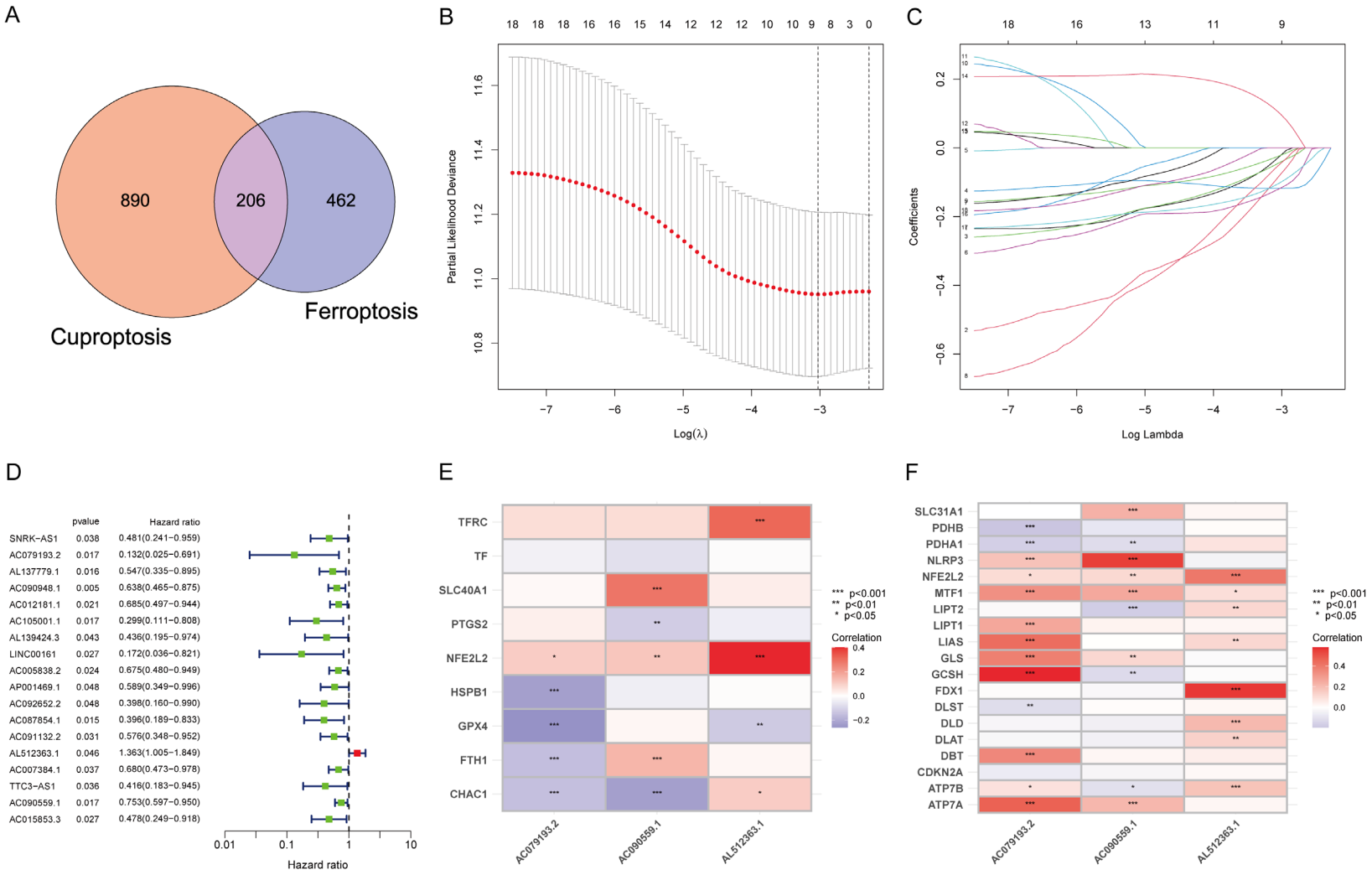

Figure 2. Screening of FCLs. (A) Venn diagram of FRLs and CRLs. (B, C) The distribution of FCLs screened by lasso-cox regression algorithm. (D) The forest diagram of 18 FCLs screened by uni-cox regression algorithm. The heatmap of three prognostic FCL and nine FRGs (E), and 19 CRGs (F).

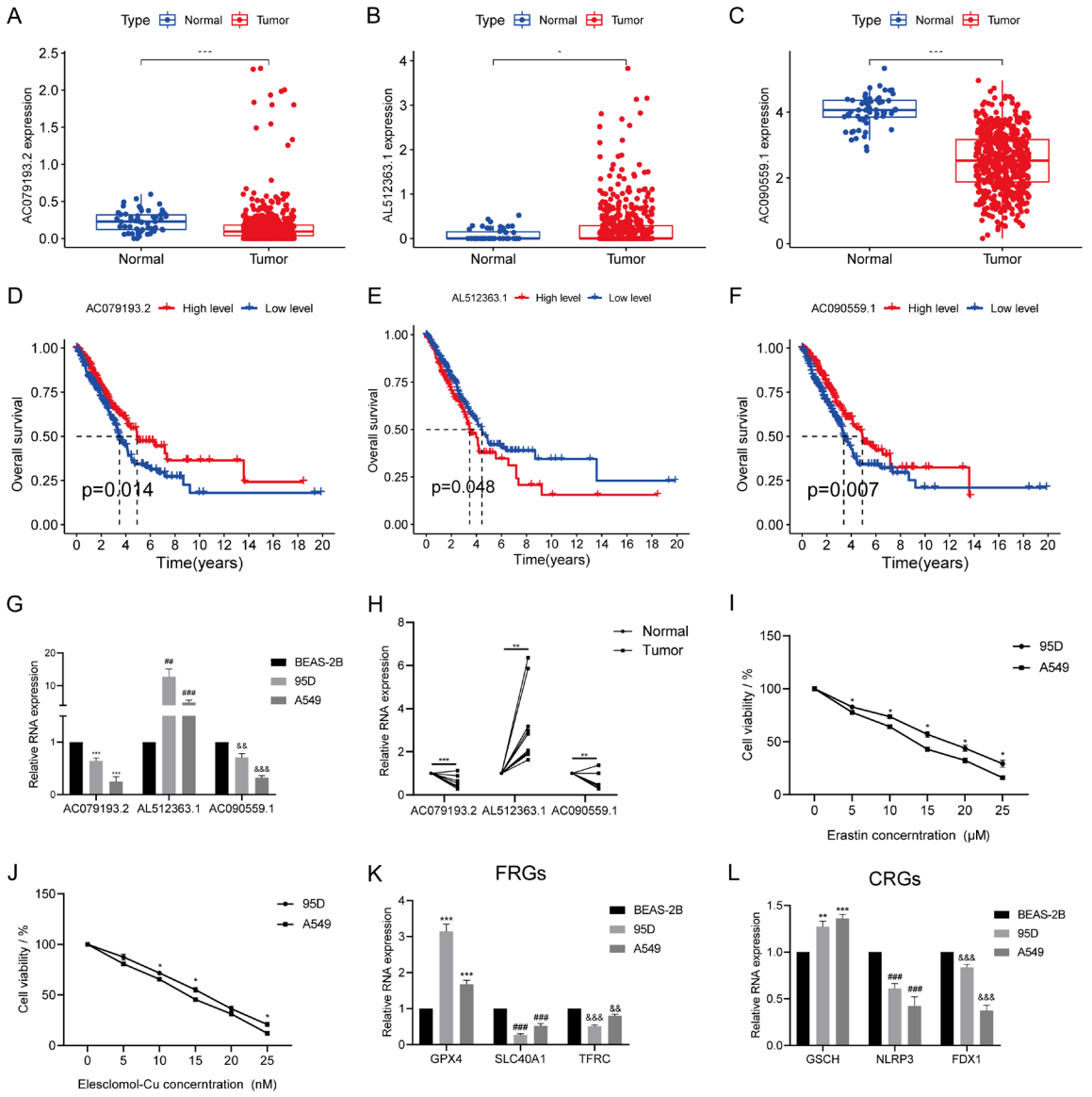

Figure 3. Expression of FCLs. A-C. Expression of three FCLs from TCGA. D-F. Survival curves of three FCLs in normal breast tissues and tumor tissues from TCGA. G, H. Expression of three FCLs three in cell lines and clinical tissues. I, J. CCK8 assay of cell sensitivity to erastin and elesclomol-Cu. K, L. Expression of FRGs and CRGs in cell lines.

CRG expression in cell lines, with similar results to the TCGA database. Compared with the normal lung cell line (BEAS-2B), GPX4 and GCSH had greater expression, and SLC40A1, TFRC, NLRP3, and FDX1 had an opposite trend in lung cancer cell lines (95D and A549) (**Figure 3K**, **3L**).

Building a prognostic risk model

We confirmed that FCLs were tumor-specific and associated with FRLs and CRLs by experimental validation. Next, we obtained clinical data from the TCGA database and randomly divided them into a training and test cohort (Supplementary Table 4), with 254 and 253 patients, respectively. According to the median expression of the risk score, each cohort was separated into high- and low-expression groups to establish a prognostic risk model. Patient risk scores (**Figure 4A-C**) and survival time (**Figure 4D-F**) are shown for the entire cohort, training cohort, and test cohort. The trends of the three FCL expressions were the same in all three groups (**Figure 4G-I**). The high-risk group was associated with a shorter OS compared to

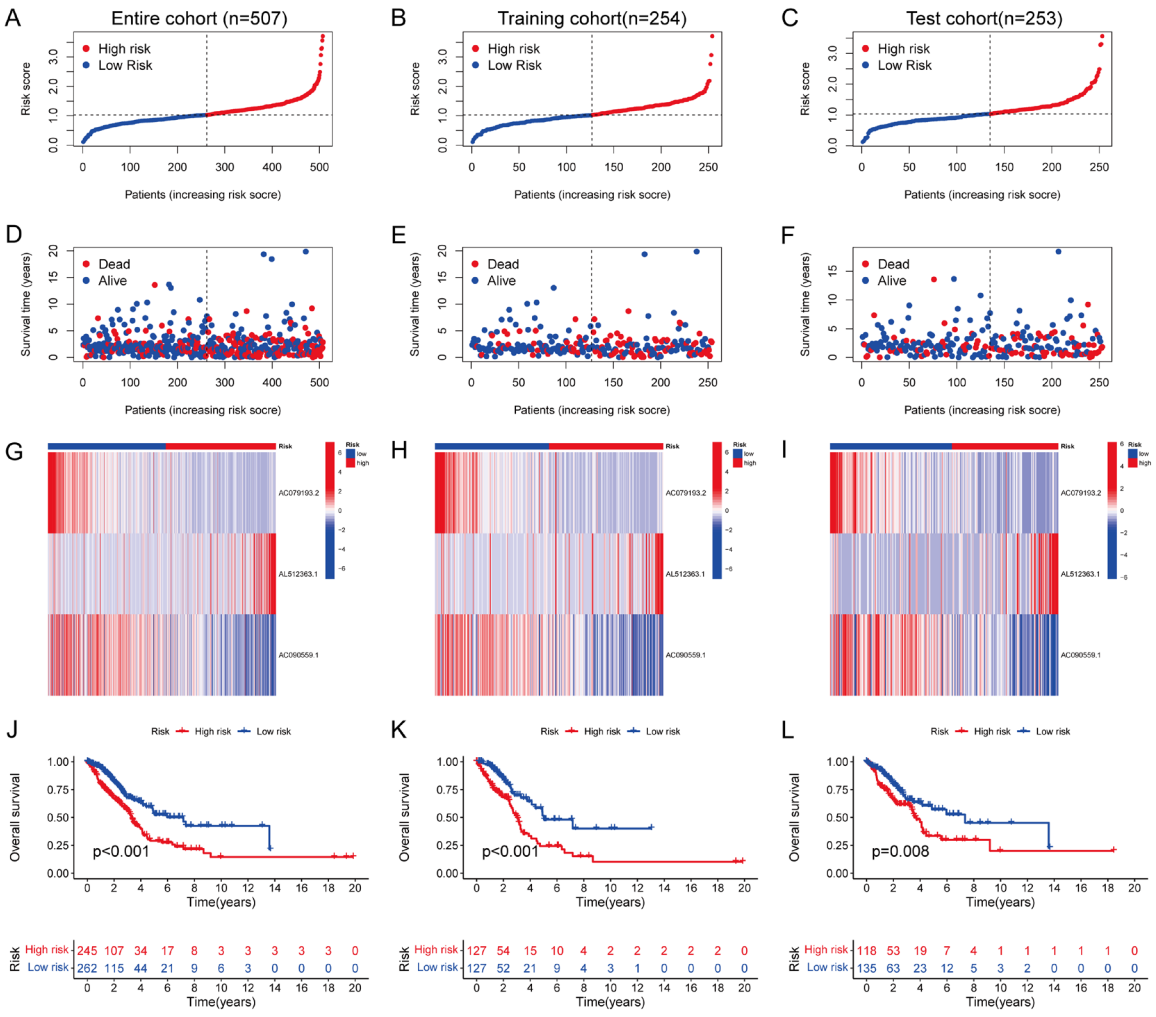

Figure 4. Construction of prognostic model. A-C. Risk score of patients in three groups. D-F. Survival status of patients in three groups. G-I. Heatmap of three FCLs in three groups. J-L. OS of patients in three groups.

the low-risk group (**Figure 4J-L**), indicating that the risk model was successfully built, and a high-risk score was associated with a poorer prognosis.

Assessment of risk model

The clinical significance of various indicators was predicted using Uni-Cox and multivariate Cox regression analyses. Five indicators, including stage, TNM classifications, and risk score, were deeply significant using Uni-Cox analysis (**Figure 5A**). Multi-Cox regression suggested a statistically significant difference between T classification and risk score; however, there were no significant differences for the remaining clinical indicators (**Figure 5B**). The accuracy of the model was analyzed using ROC and C-index curves. AUC and C-index curves estimated the accuracy of prediction for risk score, age, stage, gender, T classification, N classification, and M classification (0.691, 0.49, 0.55, 0.713, 0.652, 0.501, and 0.666, respectively) (**Figure 5C**, **5E**). The AUCs at 1-, 3-, and 5-years were estimated at 0.691, 0.579, and 0.611, respectively (**Figure 5D**). A nomogram was used to evaluate the OS (at 1-, 3-, and 5-years) of patients with LUAD. The risk score of patients was 652, and the 1-, 3-, and 5-year survival probability were estimated at 94.9%, 82.9%, and 65.8%, respectively (**Figure 5F**, **5G**). Thus, T classification and risk score were identified as independent prognostic factors for patients with LUAD.

PCA and functional annotation analyses

PCA was conducted to assess four components for both high- and low-risk subgroups. These components were as follows: all genes (**Figure**

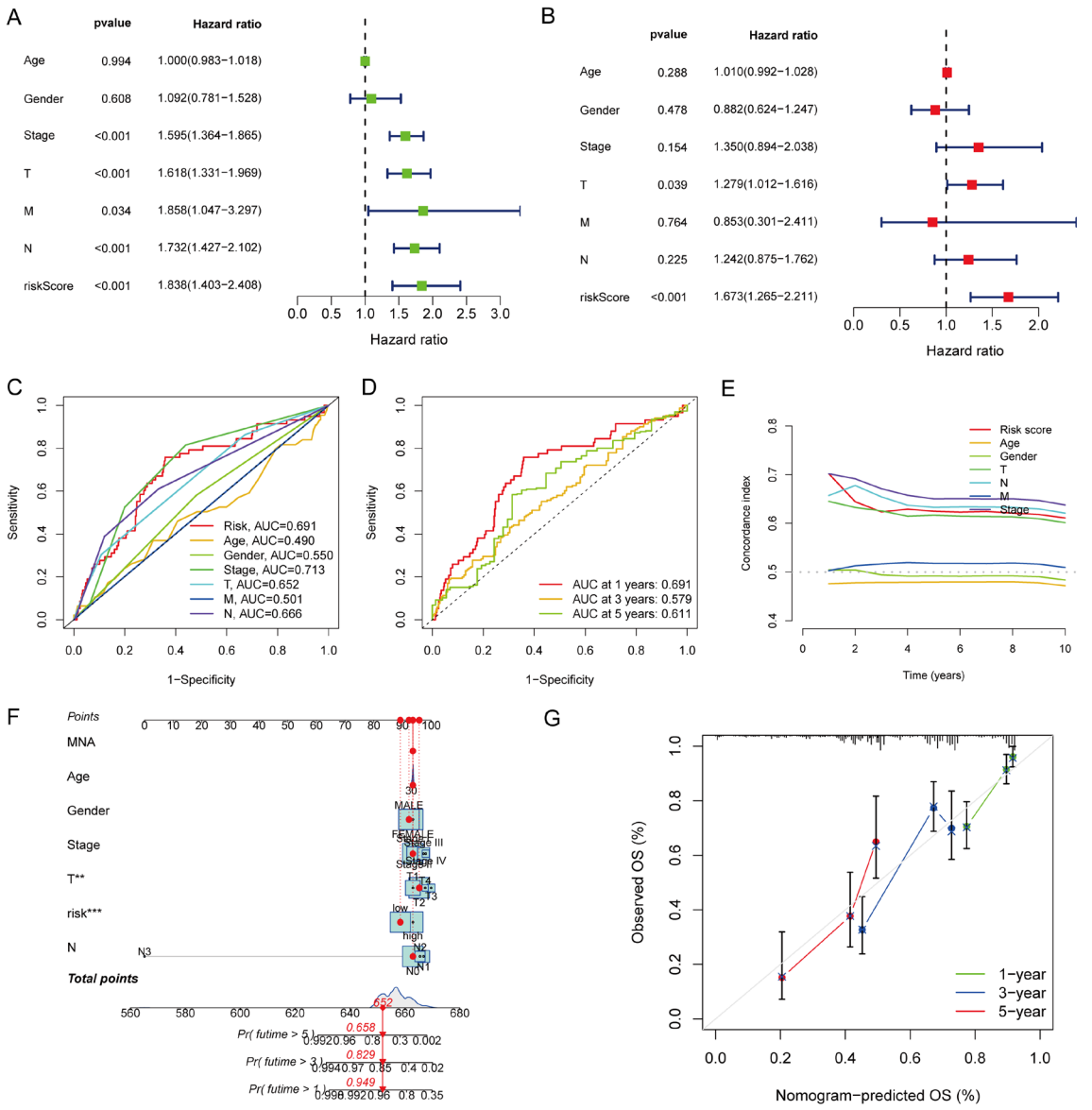

Figure 5. Prognostic evaluation of multiple clinical characteristics. Age, Gender, Stage, T classification, N classification, M classification and Risk Score were predicted by using univariate Cox analysis (A) and multivariate Cox analysis (B). (C, E) The ROC curve and C-index of clinical features. (D) The accuracy of the model prediction by ROC curve in entire set. (F, G) The nomogram predicted prognosis, and calibration tested the accuracy of prediction.

6A), CRGs and FRGs (**Figure 6B**), FCLs (**Figure 6C**), and risk-associated lncRNAs (**Figure 6D**). As shown in **Figure 6D**, the risk-associated lncRNAs constructed for the two risk groups could distinctly distinguish the two cohorts. The KEGG pathway analysis revealed 10 pathways, including hematopoietic cell lineage, primary immunodeficiency, amoebiasis, asthma, neutrophil extracellular trap formation, cell adhesion molecules, leishmaniasis, staphylococcus aureus infection, complement and coagulation cascades, and allograft rejection (**Figure 6E**). GO analysis revealed that the FCLs were related to immune responses and NADP+ activity, such as NADP activity, T cell receptor complex, and immune response-regulating signaling pathway (**Figure 6F**; Supplementary Table 5).

Exploration of the immune landscape

We used five different methods (TIMER, CIBERSORT, CIBERSORT-ABS, QUANTISEQ, MCPCOUNTER, XCELL, and EPIC) to predict the correlation between the two risk groups and

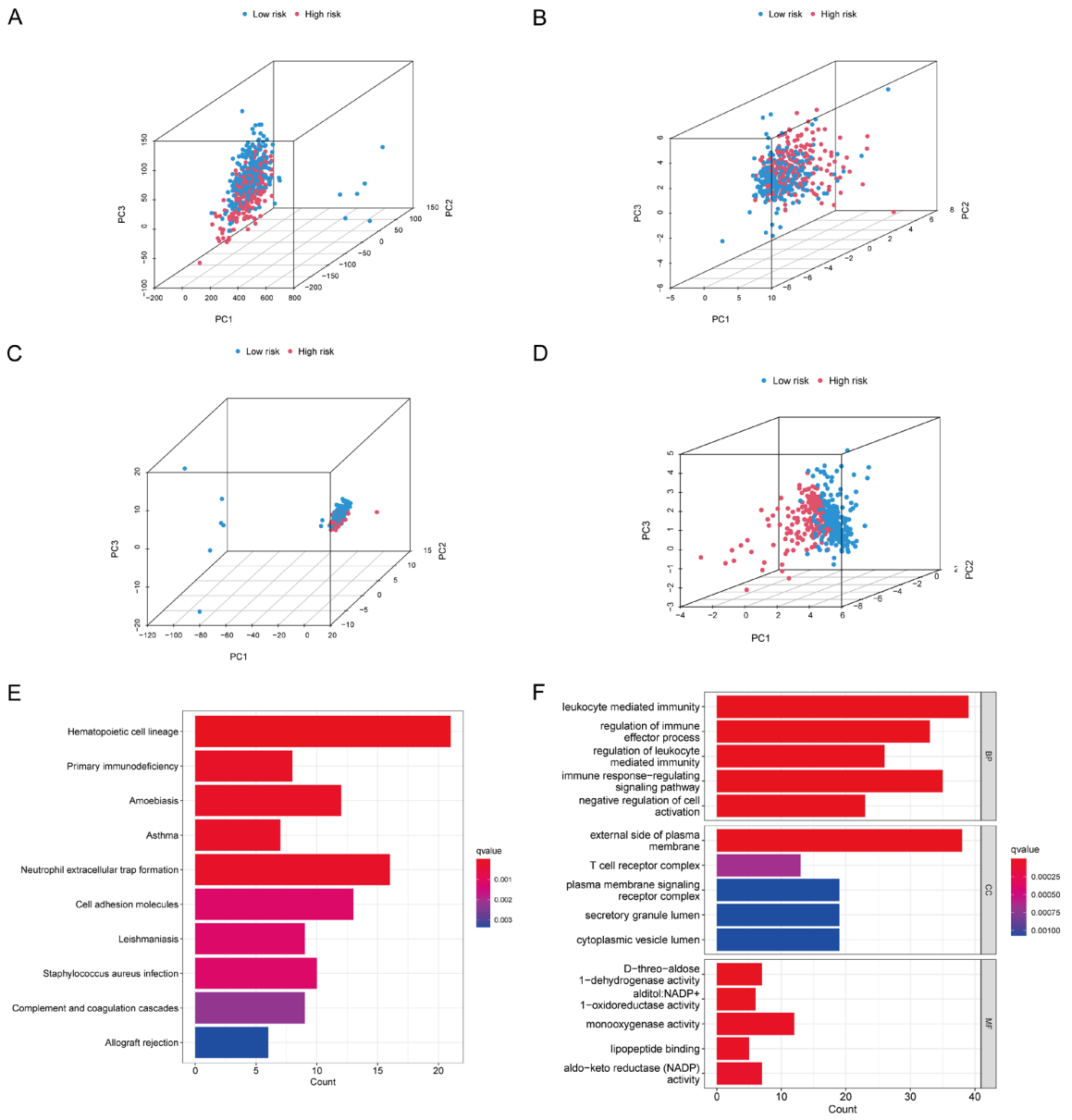

Figure 6. PCA and functional annotations. PCA of (A) All genes. (B) FRGs and CRGs. (C) FCLs. (D) Risk lncRNAs. Loop diagram of (E) KEGG pathway and (F) GO analyses.

immune cells, which revealed that B cell and T cell CD4+ (common part) had significant associations in both risk cohorts (**Figure 7A**). As presented in **Figure 7B**, we observed a strong association between FCLs and immune functions in the two risk groups. These immune functions included type II Interferon (IFN) response ($P < 0.001$), type I IFN response ($P < 0.05$), HLA ($P < 0.001$), APC co-stimulation ($P < 0.001$), APC co-inhibition ($P < 0.001$), CCR ($P < 0.001$), parainflammation ($P < 0.001$), MHC class I ($P < 0.05$), cytolytic activity ($P < 0.01$), inflammation-promoting ($P < 0.01$), check-point ($P < 0.001$), and T cell co-stimulation ($P < 0.001$). In addition, we assessed the correlation between m6A-related gene expression and risk groups and found eight genes (YTHDC2, RBM15, HNRNPC, YTHDC1, FTO, METTL3, METTL14, and ZC3H13) associated with risk cohorts (**Figure 7C**). Finally, the analysis in **Figure 7D** indicated that 43 immune checkpoints ($P < 0.05$) were associated with FCLs in high- and low-risk groups.

Discussion

LUAD is one of the most common malignant tumors with high incidence and mortality world-

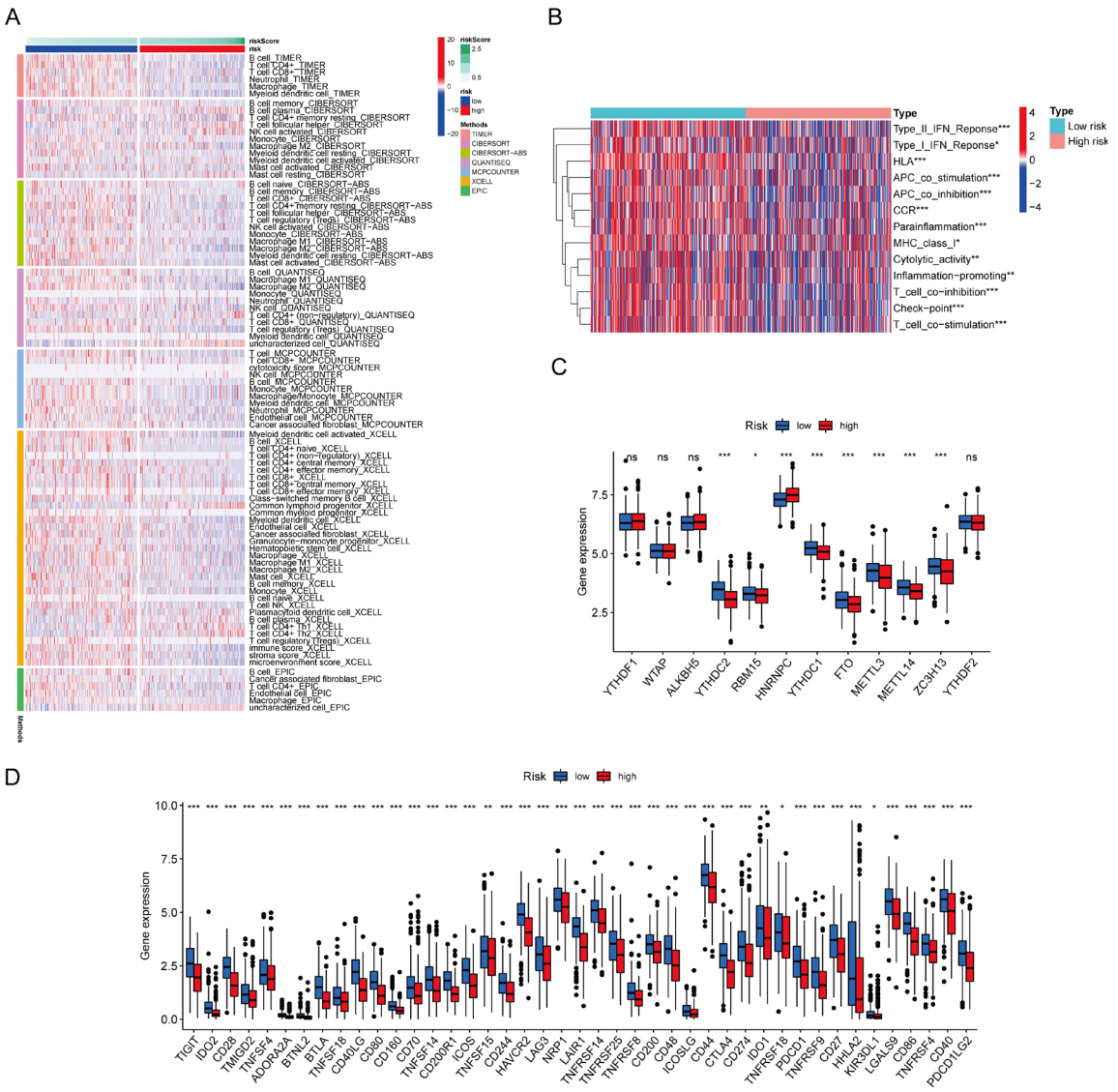

Figure 7. Immune-related functional introduction. A. The fraction of immune cells between the two risk cohorts using seven methods. B. Immune function of two risk groups. C. m6A-related genes expression between the two risk cohorts. D. Expression of immune checkpoints.

wide [1]. Ferroptosis, a phenomenon first reported in 2012, and cuproptosis, a newly recognized process in 2022 [5, 12], are distinct forms of cell death. Each type has its own unique inducers, e.g., erastin for ferroptosis and elesclomol-Cu (II) for cuproptosis [7, 11]. Furthermore, lncRNAs are associated with ferroptosis and cuproptosis [17, 18]; however, the mechanism of FCLs in tumors, especially in LUAD, is still unclear. Therefore, investigating the role of FCLs and their use in the construction of a risk model might provide a new therapeutic direction for patients with LUAD.

Risk models of FRL have been reported in the published literature [19-22]; likewise, prognostic models of CRL can also be found in the published study [23-26]. However, an FCL-related prognostic model has not been reported. Herein, we first identified three FCLs (*AC079193.2*, *AC090559.1*, and *AL512363.1*) for LUAD through the LASSO-Cox algorithm based on the TCGA database. After we confirmed that FCLs were tumor-specific and relevant to ferroptosis and cuproptosis, a prognostic risk model was established. The results showed that the risk score and T classification

could serve as independent prognostic parameters. A nomogram was used to assess the OS for patients with LUAD, which might act as a supplementary prediction tool. Next, we also found that there were strong internal connections between risk cohorts and multiple immune functions, immune cells, as well as m6A-related genes, and especially immune checkpoints. Finally, the correlation between the risk groups and drug sensitivity was computed. The data showed that risk scores were negative with six clinical drugs for LUAD. Taken together, the FCL signature could potentially predict the prognosis of patients with LUAD, with high-risk scores linked to poorer OS.

Among the three FCLs used in the risk score, high-risk lncRNA *AL512363.1* was linked to a worse prognosis, whereas the low-risk lncRNAs *AC079193.2* and *AC090559.1* with associated with better OS. Notably, *AC090559.1* is a ferroptosis- and pyroptosis-related lncRNA that could predict patient prognosis for LUAD [19, 27]. In other studies, *AC090559.1* has also been identified as a necroptosis-related lncRNA that is down-regulated in osteosarcoma, and associated with a poor prognosis [28]. In contrast, *AC079193.2* and *AL512363.1* have not been studied.

In this study, we detected the expression of three FRGs and three CRGs in two cell lines. Among these genes, *GPX4* plays a crucial role in ferroptosis, and its protein levels can be inhibited through MTORC1 using drugs, thus enhancing the susceptibility of lung cancer cells to ferroptosis [29]. Notably, Jia et al. proved that *GPX4* activated the cGAS-STING signaling pathway and modulated STING-dependent immunopathology [30]. *SLC40A1*, on the other hand, is an iron transporter that plays an essential role in early embryonic development [31]. Overexpression of *TFRC* in neuroblastoma cells induces sensitivity to ferroptosis [32]. Cuproptosis-related *FDX1*, acting as the direct target of elesclomol, could rescue copper-independent cell death [33]. *NLRP3* could lead to the formation of a complex that was the platform of caspase-1 activation and mediating the release of IL-1β, IL-18, and GSDMD-induced cell death [34]. Lastly, the protein-coding transcript variant 1 of *GCSH*, when overexpressed, imparts an additional increase in vitality to breast cancer cells [35].

The tumor immune microenvironment is recognized as a significant factor in cancer development and is central to immunotherapy [36]. GO analysis revealed that FCLs were related to immune response and NADP+ activity; however, there was no direct link to ferroptosis or cuproptosis. This could be due to the moderate Pearson correlation coefficient of 0.4 among the screen lncRNA, indicating that their correlation might not be very strong. The FCL risk model, however, was strongly associated with multiple immune functions, including IFN responses, HLA, MHC class I, and immune checkpoints. IFN response determines dynamic tumor-immune interaction in the process of cancer development and metastasis. IFN also plays a dual role leading to immune checkpoint blockade response [37]. The degree of heterozygosity in the HLA gene family was correlated with survival probability in patients with non-small-cell lung cancer treated with immune checkpoint inhibition [38]. In 2019, Burr et al. proved that the deletion of MHC class I in multiple tumor cells could decrease immunotherapy sensitivity [39]. In our data, immune checkpoints like PD1 and CTLA4 were more active in the low-risk group than in the high-risk group. Previous research has shown that CTAL4 treatment can reverse tumor growth mediated by CD4 T cytotoxicity [40]. In the past decade, anti-PD1/PDL1 immunotherapy has become the standard treatment for stage III-IV non-small-cell lung cancer [41].

Furthermore, the analysis involving five methods to assess the relationship between risk groups and immune cells suggested that seven immune cells, including B cells, T cells, natural killer (NK) cells, monocytes, macrophages, myeloid dendritic cells, and mast cells, had significant associations with risk groups. These immune cells have been implicated in various aspects of tumor immunity, such as memory T cell metabolism improvement [42]; mature dendritic cell activation and migration [43]; NK cell involvement in immunotherapy [44]; antibody production of B cells involved in resistance to severe acute respiratory syndrome coronavirus 2 invasions [45]; and the dual role of macrophages in pathogen neutralization and immune response modulation [46]. Finally, the analysis of m6A-related genes in relation to the risk cohorts revealed that eight genes had higher expression in the low-risk

group compared to the high-risk group. M6A-related genes and lncRNAs are known to be associated with ferroptosis and cuproptosis [47, 48]. It has also been shown that cisplatin and doxorubicin, common anti-cancer drugs, had higher sensitivity in low-risk groups compared to high-risk groups. Kuerban et al. proved that doxorubicin-loaded bacterial outer-membrane could improve anti-cancer efficacy to obviously decrease side effects [49].

This study does have a few limitations. First, the data used for analysis was only obtained from the TCGA database, and further research involving a clinical cohort would be beneficial. Second, experimental validation and in vivo studies are lacking, which would provide a deeper understanding of the mechanisms involved.

In conclusion, this study confirmed the tumor-specific nature of three screened FCLs, namely *AC079193.2*, *AC090559.1*, and *AL512363.1*, and established their relevance to ferroptosis and cuproptosis. By integrating these cell death processes, a prognostic risk model was constructed. This model was able to predict patient OS and assess the immune microenvironment. Our findings might provide a potential opportunity for clinical applications in patients with LUAD.

Acknowledgements

We appreciate the support of Shandong Provincial Hospital and Shandong First Medical University. The research was supported by National Natural Science Foundation of China (Grant No. 8197102168). We thank Bullet Edits Limited for editing the language of the manuscript.

Disclosure of conflict of interest

None.

Address correspondence to: Xiaoyan Lin, Department of Pathology, Shandong Provincial Hospital Affiliated to Shandong First Medical University, Jinan, Shandong, China. E-mail: linxiaoyanyan@163.com; Pengju Zhang, Department of Biochemistry and Molecular Biology, School of Basic Medical Sciences, Cheeloo College of Medicine, Shandong University, Jinan, Shandong, China. E-mail: zhpj@sdu.edu.cn

References

[1] Siegel RL, Miller KD, Fuchs HE and Jemal A. Cancer statistics, 2022. CA Cancer J Clin 2022; 72: 7-33.

[2] Howlader N, Forjaz G, Mooradian MJ, Meza R, Kong CY, Cronin KA, Mariotto AB, Lowy DR and Feuer EJ. The effect of advances in lung-cancer treatment on population mortality. N Engl J Med 2020; 383: 640-649.

[3] Lin W, Chen Y, Wu B, Chen Y and Li Z. Identification of the pyroptosis-related prognostic gene signature and the associated regulation axis in lung adenocarcinoma. Cell Death Discov 2021; 7: 161.

[4] Tan AC and Tan DSW. Targeted therapies for lung cancer patients with oncogenic driver molecular alterations. J Clin Oncol 2022; 40: 611-625.

[5] Dixon SJ. Ferroptosis: bug or feature? Immunol Rev 2017; 277: 150-157.

[6] Chen X, Kang R, Kroemer G and Tang D. Ferroptosis in infection, inflammation, and immunity. J Exp Med 2021; 218: e20210518.

[7] Mou Y, Wang J, Wu J, He D, Zhang C, Duan C and Li B. Ferroptosis, a new form of cell death: opportunities and challenges in cancer. J Hematol Oncol 2019; 12: 34.

[8] Xie Y, Hou W, Song X, Yu Y, Huang J, Sun X, Kang R and Tang D. Ferroptosis: process and function. Cell Death Differ 2016; 23: 369-379.

[9] Cobine PA and Brady DC. Cuproptosis: cellular and molecular mechanisms underlying copper-induced cell death. Mol Cell 2022; 82: 1786-1787.

[10] Li SR, Bu LL and Cai L. Cuproptosis: lipoylated TCA cycle proteins-mediated novel cell death pathway. Signal Transduct Target Ther 2022; 7: 158.

[11] Gao W, Huang Z, Duan J, Nice EC, Lin J and Huang C. Elesclomol induces copper-dependent ferroptosis in colorectal cancer cells via degradation of ATP7A. Mol Oncol 2021; 15: 3527-3544.

[12] Tsvetkov P, Coy S, Petrova B, Dreishpoon M, Verma A, Abdusamad M, Rossen J, Joesch-Cohen L, Humeidi R, Spangler RD, Eaton JK, Frenkel E, Kocak M, Corsello SM, Lutsenko S, Kanarek N, Santagata S and Golub TR. Copper induces cell death by targeting lipoylated TCA cycle proteins. Science 2022; 375: 1254-1261.

[13] Borsani G, Tonlorenzi R, Simmler MC, Dandolo L, Arnaud D, Capra V, Grompe M, Pizzuti A, Muzny D, Lawrence C, Willard HF, Avner P and Ballabio A. Characterization of a murine gene expressed from the inactive X chromosome. Nature 1991; 351: 325-329.

[14] Bridges MC, Daulagala AC and Kourtidis A. LNCcation: lncRNA localization and function. J Cell Biol 2021; 220: e202009045.
[15] Singh D, Assaraf YG and Gacche RN. Long non-coding RNA mediated drug resistance in breast cancer. Drug Resist Updat 2022; 63: 100851.
[16] Liu T, Han C, Fang P, Ma Z, Wang X, Chen H, Wang S, Meng F, Wang C, Zhang E, Dong G, Zhu H, Yin W, Wang J, Zuo X, Qiu M, Wang J, Qian X, Shen H, Xu L, Hu Z and Yin R. Cancer-associated fibroblast-specific lncRNA LINC-01614 enhances glutamine uptake in lung adenocarcinoma. J Hematol Oncol 2022; 15: 141.
[17] Tang R, Wu Z, Rong Z, Xu J, Wang W, Zhang B, Yu X and Shi S. Ferroptosis-related lncRNA pairs to predict the clinical outcome and molecular characteristics of pancreatic ductal adenocarcinoma. Brief Bioinform 2022; 23: bbab388.
[18] Tang L, Wang T, Li W, Yu S, Yao S and Cheng H. Construction of cuproptosis-related lncRNAs/mRNAs model and prognostic prediction of hepatocellular carcinoma. Am J Cancer Res 2022; 12: 4693-4707.
[19] Guo Y, Qu Z, Li D, Bai F, Xing J, Ding Q, Zhou J, Yao L and Xu Q. Identification of a prognostic ferroptosis-related lncRNA signature in the tumor microenvironment of lung adenocarcinoma. Cell Death Discov 2021; 7: 190.
[20] Lu L, Liu LP, Zhao QQ, Gui R and Zhao QY. Identification of a ferroptosis-related LncRNA signature as a novel prognosis model for lung adenocarcinoma. Front Oncol 2021; 11: 675545.
[21] Wang Y, Lu G, Xue X, Xie M, Wang Z, Ma Z, Feng Y, Shao C, Duan H, Pan M, Ding P, Li X, Han J and Yan X. Characterization and validation of a ferroptosis-related LncRNA signature as a novel prognostic model for lung adenocarcinoma in tumor microenvironment. Front Immunol 2022; 13: 903758.
[22] Bi G, Liang J, Zhao M, Zhang H, Jin X, Lu T, Zheng Y, Bian Y, Chen Z, Huang Y, Besskaya V, Zhan C, Wang Q and Tan L. miR-6077 promotes cisplatin/pemetrexed resistance in lung adenocarcinoma via CDKN1A/cell cycle arrest and KEAP1/ferroptosis pathways. Mol Ther Nucleic Acids 2022; 28: 366-386.
[23] Mo X, Hu D, Yang P, Li Y, Bashir S, Nai A, Ma F, Jia G and Xu M. A novel cuproptosis-related prognostic lncRNA signature and lncRNA MIR31HG/miR-193a-3p/TNFRSF21 regulatory axis in lung adenocarcinoma. Front Oncol 2022; 12: 927706.
[24] Wang Z, Yao J, Dong T and Niu X. Definition of a novel cuproptosis-relevant lncRNA signature for uncovering distinct survival, genomic alterations, and treatment implications in lung adenocarcinoma. J Immunol Res 2022; 2022: 2756611.
[25] Wang S, Xing N, Meng X, Xiang L and Zhang Y. Comprehensive bioinformatics analysis to identify a novel cuproptosis-related prognostic signature and its ceRNA regulatory axis and candidate traditional Chinese medicine active ingredients in lung adenocarcinoma. Front Pharmacol 2022; 13: 971867.
[26] Ma S, Zhu J, Wang M, Zhu J, Wang W, Xiong Y, Jiang R, Seetharamu N, Abrao FC, Puthamohan VM, Liu L and Jiang T. A cuproptosis-related long non-coding RNA signature to predict the prognosis and immune microenvironment characterization for lung adenocarcinoma. Transl Lung Cancer Res 2022; 11: 2079-2093.
[27] Liu J, Liu Q, Shen H, Liu Y, Wang Y, Wang G and Du J. Identification and validation of a three pyroptosis-related lncRNA signature for prognosis prediction in lung adenocarcinoma. Front Genet 2022; 13: 838624.
[28] Zheng Y, Xu J, Lin J and Lin Y. A novel necroptosis-related lncRNA signature for osteosarcoma. Comput Math Methods Med 2022; 2022: 8003525.
[29] Zhang Y, Swanda RV, Nie L, Liu X, Wang C, Lee H, Lei G, Mao C, Koppula P, Cheng W, Zhang J, Xiao Z, Zhuang L, Fang B, Chen J, Qian SB and Gan B. mTORC1 couples cyst(e)ine availability with GPX4 protein synthesis and ferroptosis regulation. Nat Commun 2021; 12: 1589.
[30] Jia M, Qin D, Zhao C, Chai L, Yu Z, Wang W, Tong L, Lv L, Wang Y, Rehwinkel J, Yu J and Zhao W. Redox homeostasis maintained by GPX4 facilitates STING activation. Nat Immunol 2020; 21: 727-735.
[31] Donovan A, Lima CA, Pinkus JL, Pinkus GS, Zon LI, Robine S and Andrews NC. The iron exporter ferroportin/Slc40a1 is essential for iron homeostasis. Cell Metab 2005; 1: 191-200.
[32] Lu Y, Yang Q, Su Y, Ji Y, Li G, Yang X, Xu L, Lu Z, Dong J, Wu Y, Bei JX, Pan C, Gu X and Li B. MYCN mediates TFRC-dependent ferroptosis and reveals vulnerabilities in neuroblastoma. Cell Death Dis 2021; 12: 511.
[33] Tsvetkov P, Detappe A, Cai K, Keys HR, Brune Z, Ying W, Thiru P, Reidy M, Kugener G, Rossen J, Kocak M, Kory N, Tsherniak A, Santagata S, Whitesell L, Ghobrial IM, Markley JL, Lindquist S and Golub TR. Mitochondrial metabolism promotes adaptation to proteotoxic stress. Nat Chem Biol 2019; 15: 681-689.
[34] Wang L and Hauenstein AV. The NLRP3 inflammasome: Mechanism of action, role in disease and therapies. Mol Aspects Med 2020; 76: 100889.
[35] Adamus A, Muller P, Nissen B, Kasten A, Timm S, Bauwe H, Seitz G and Engel N. GCSH anti-

sense regulation determines breast cancer cells' viability. Sci Rep 2018; 8: 15399.
[36] Bejarano L, Jordao MJC and Joyce JA. Therapeutic targeting of the tumor microenvironment. Cancer Discov 2021; 11: 933-959.
[37] von Locquenghien M, Rozalen C and Celia-Terrassa T. Interferons in cancer immunoediting: sculpting metastasis and immunotherapy response. J Clin Invest 2021; 131: e143296.
[38] Naranbhai V, Viard M, Dean M, Groha S, Braun DA, Labaki C, Shukla SA, Yuki Y, Shah P, Chin K, Wind-Rotolo M, Mu XJ, Robbins PB, Gusev A, Choueiri TK, Gulley JL and Carrington M. HLA-A*03 and response to immune checkpoint blockade in cancer: an epidemiological biomarker study. Lancet Oncol 2022; 23: 172-184.
[39] Burr ML, Sparbier CE, Chan KL, Chan YC, Kersbergen A, Lam EYN, Azidis-Yates E, Vassiliadis D, Bell CC, Gilan O, Jackson S, Tan L, Wong SQ, Hollizeck S, Michalak EM, Siddle HV, McCabe MT, Prinjha RK, Guerra GR, Solomon BJ, Sandhu S, Dawson SJ, Beavis PA, Tothill RW, Cullinane C, Lehner PJ, Sutherland KD and Dawson MA. An evolutionarily conserved function of polycomb silences the MHC class I antigen presentation pathway and enables immune evasion in cancer. Cancer Cell 2019; 36: 385-401, e8.
[40] Miggelbrink AM, Jackson JD, Lorrey SJ, Srinivasan ES, Waibl-Polania J, Wilkinson DS and Fecci PE. CD4 T-cell exhaustion: does it exist and what are its roles in cancer? Clin Cancer Res 2021; 27: 5742-5752.
[41] Dantoing E, Piton N, Salaun M, Thiberville L and Guisier F. Anti-PD1/PD-L1 immunotherapy for non-small cell lung cancer with actionable oncogenic driver mutations. Int J Mol Sci 2021; 22: 6288.
[42] Corrado M and Pearce EL. Targeting memory T cell metabolism to improve immunity. J Clin Invest 2022; 132: e148546.
[43] Bol KF, Schreibelt G, Gerritsen WR, de Vries IJ and Figdor CG. Dendritic cell-based immunotherapy: state of the art and beyond. Clin Cancer Res 2016; 22: 1897-1906.
[44] Kundu S, Gurney M and O'Dwyer M. Generating natural killer cells for adoptive transfer: expanding horizons. Cytotherapy 2021; 23: 559-566.
[45] Roltgen K and Boyd SD. Antibody and B cell responses to SARS-CoV-2 infection and vaccination. Cell Host Microbe 2021; 29: 1063-1075.
[46] Sheu KM and Hoffmann A. Functional hallmarks of healthy macrophage responses: their regulatory basis and disease relevance. Annu Rev Immunol 2022; 40: 295-321.
[47] Gao C, Kong N, Zhang F, Zhou L, Xu M and Wu L. Development and validation of the potential biomarkers based on m6A-related lncRNAs for the predictions of overall survival in the lung adenocarcinoma and differential analysis with cuproptosis. BMC Bioinformatics 2022; 23: 327.
[48] Yang H, Hu Y, Weng M, Liu X, Wan P, Hu Y, Ma M, Zhang Y, Xia H and Lv K. Hypoxia inducible lncRNA-CBSLR modulates ferroptosis through m6A-YTHDF2-dependent modulation of CBS in gastric cancer. J Adv Res 2021; 37: 91-106.
[49] Kuerban K, Gao X, Zhang H, Liu J, Dong M, Wu L, Ye R, Feng M and Ye L. Doxorubicin-loaded bacterial outer-membrane vesicles exert enhanced anti-tumor efficacy in non-small-cell lung cancer. Acta Pharm Sin B 2020; 10: 1534-1548.

Supplementary Table 1. The information of primers

Name	Primer	Sequence	Tm/°C	Size/bp
GAPDH	Forward	GCACCGTCAAGGCTGAGAAC	59.50	138
	Reverse	TGGTGAAGACGCCAGTGGA	57.30	
AL512363.1	Forward	CCTCTGTCTCACTTCAGCTGTT	57.67	74
	Reverse	TGATTGGAAAACAAGACGCTGG	55.81	
AC079193.2	Forward	ACAGCATAGTCTGCCCCTTTG	57.57	70
	Reverse	TGTATGGCATTCAAGTGTGCGT	55.81	
AC090559.1	Forward	CACGCAGAGGAGCACG	56.84	177
	Reverse	ATCGTGCTGGAATGTGGCT	55.16	
GPX4	Forward	CAGTGAGGCAAGACCGAAGT	57.45	104
	Reverse	CCGAACTGGTTACACGGGAA	57.45	
SLC40A1	Forward	ACTGTCCTGGGCTTTGACTG	57.45	163
	Reverse	GACCTGTCCGAACCAAACCA	57.45	
TFRC	Forward	AACTCAGCAAAGTCTGGCGT	55.40	137
	Reverse	ATACGCCACATAACCCCCAG	57.45	
FDX1	Forward	TTGGTGCATGTGAGGGAACC	57.45	145
	Reverse	CCCAACCGTGATCTGTCTGT	57.45	
NLRP3	Forward	GAGCCGAAGTGGGGTTCAGA	59.5	73
	Reverse	CTTCAATGCTGTCTTCCTGGC	57.57	
GCSH	Forward	GCGCCGTCCGTACGCT	59.40	136

Supplementary Table 2. The correlation between FRGs and FCLs

FRGs	LncRNA	Cor	*P*-value	Regulation
GPX4	SNRK-AS1	-0.2513	3.29E-09	Negative
GPX4	AC079193.2	-0.2590	1.03E-09	Negative
GPX4	AL137779.1	-0.2571	1.39E-09	Negative
GPX4	AC090948.1	-0.2577	1.26E-09	Negative
GPX4	AC012181.1	-0.2704	1.75E-10	Negative
GPX4	AC105001.1	-0.2653	3.90E-10	Negative
GPX4	AC015853.3	-0.2526	2.73E-09	Negative
GPX4	LINC00161	-0.2517	3.13E-09	Negative
GPX4	AC005838.2	-0.2592	1.00E-09	Negative
GPX4	AP001469.1	-0.2505	3.73E-09	Negative
GPX4	AC092652.2	-0.2539	2.23E-09	Negative
GPX4	AC087854.1	-0.2766	6.39E-11	Negative
GPX4	AC091132.2	-0.2560	1.63E-09	Negative
GPX4	AC007384.1	-0.2670	3.01E-10	Negative
GPX4	TTC3-AS1	-0.2520	2.99E-09	Negative
SLC40A1	AC090559.1	0.2845	1.70E-11	Positive
TFRC	AL512363.1	0.3141	8.26E-14	Positive
HSPB1	AL139424.3	-0.2517	3.12E-09	Negative

Supplementary Table 3. The correlation between CRGs and FCLs

CRGs	LncRNA	Cor	*P*-value	Regulation
GCSH	SNRK-AS1	0.5318	1.11E-40	Positive
GCSH	AC079193.2	0.5812	8.22E-50	Positive
GCSH	AL137779.1	0.5499	6.51E-44	Positive
GCSH	AC090948.1	0.5742	1.34E-48	Positive
GCSH	AC012181.1	0.5407	3.01E-42	Positive
GCSH	AC105001.1	0.5325	8.30E-41	Positive
GCSH	TTC3-AS1	0.5844	1.13E-50	Positive
GCSH	AC007384.1	0.5239	2.49E-39	Positive
GCSH	LINC00161	0.5081	1.01E-36	Positive
GCSH	AC005838.2	0.5478	1.57E-43	Positive
GCSH	AP001469.1	0.5745	1.17E-48	Positive
GCSH	AC092652.2	0.5340	4.53E-41	Positive
GCSH	AC087854.1	0.5633	1.87E-46	Positive
GCSH	AC091132.2	0.5121	2.28E-37	Positive
FDX1	AL512363.1	0.5588	1.37E-45	Positive
NLRP3	AC090559.1	0.5489	9.68E-44	Positive
GCSH	AC015853.3	0.5562	4.25E-45	Positive
ATP7A	AL139424.3	0.5154	6.50E-38	Positive

Supplementary Table 4. The patient's clinical features of three groups

Covariates	Type	Total	Test	Train	*P*-value
Age	≤ 65	239 (47.14%)	118 (46.64%)	121 (47.64%)	0.8915
	> 65	258 (50.89%)	130 (51.38%)	128 (50.39%)	
	Unknow	10 (1.97%)	5 (1.98%)	5 (1.97%)	
Gender	FEMALE	272 (53.65%)	139 (54.94%)	133 (52.36%)	0.622
	MALE	235 (46.35%)	114 (45.06%)	121 (47.64%)	
Stage	Stage I	272 (53.65%)	133 (52.57%)	139 (54.72%)	0.8553
	Stage II	120 (23.67%)	59 (23.32%)	61 (24.02%)	
	Stage III	81 (15.98%)	41 (16.21%)	40 (15.75%)	
	Stage IV	26 (5.13%)	15 (5.93%)	11 (4.33%)	
	Unknow	8 (1.57%)	5 (1.97%)	3 (1.18%)	
T	T1	169 (33.33%)	82 (32.41%)	87 (34.25%)	0.2243
	T2	271 (53.45%)	144 (56.92%)	127 (50%)	
	T3	45 (8.88%)	17 (6.72%)	28 (11.02%)	
	T4	19 (3.75%)	8 (3.16%)	11 (4.33%)	
	Unknow	3 (0.59%)	2 (0.79%)	1 (0.40%)	
M	M0	338 (66.67%)	170 (67.19%)	168 (66.14%)	0.7315
	M1	25 (4.93%)	14 (5.53%)	11 (4.33%)	
	Unknow	144 (28.4%)	69 (27.28%)	75 (29.53%)	
N	N0	327 (64.5%)	159 (62.85%)	168 (66.14%)	0.4136
	N1	95 (18.74%)	50 (19.76%)	45 (17.72%)	
	N2	71 (14%)	38 (15.02%)	33 (12.99%)	
	N3	2 (0.39%)	0 (0%)	2 (0.79%)	
	Unknow	12 (2.37%)	6 (2.37%)	6 (2.36%)	